Optimal Cell Reconstruction of 3D Foam Images

André E. Liebscher* and Claudia Redenbach*
*Department of Mathematics, University of Kaiserslautern, Kaiserslautern, Germany
Email: {liebscher, redenbach}@mathematik.uni-kl.de

***Abstract*—The watershed based cell reconstruction is a common approach to segment the cell system of foams and polycrystals. To avoid segmentation errors, a proper parametrisation of the algorithm is necessary. In this work, we propose a marker based method whose parameters are automatically adapted to the observed structure. The result is a nearly perfect cell reconstruction with segmentation errors below one percent.**

I. Introduction

An open cell foam is a subdivision of space into random polyhedral cells whose struts form an interconnected network. The macroscopic properties of an open cell foam are highly influenced by the microstructure of the foam. Recent research indicates that this complex relation can be studied by an exact characterisation of the microstructure followed by numeric simulations [1], [2], [3]. The key element of such a study is the microstructure model of the foam.

The physical laws behind the formation of a foam lead to random Laguerre tessellations as suitable model for the cell system of a foam [4, Chap. 3]. A Laguerre tessellation is a subdivision of space into polyhedral cells $C([x,r],\varphi) = \big\{z \in \mathbb{R}^3 \mid \operatorname{pow}(z,[x,r]) \leq \operatorname{pow}(z,[x',r']),\ [x',r'] \in \varphi\big\}$ formed by a locally finite set of spheres $[x,r] \in \varphi$ (with centre $x \in \mathbb{R}^3$ and radius $r \in \mathbb{R}_+$) that interact through the power distance $\operatorname{pow}(z,[x,r]) = \|z-x\|^2 - r^2$. If all radii are equal, we obtain the well known Voronoi tessellation as special case.

To fit a Laguerre tessellation to the cell system of a foam, empirical distributions of cell size and shape are necessary. These characteristics are typically estimated from a μCT image of the foam using the cell reconstruction procedure described in [5]. This procedure divides the pore space of the foam into cells whose edges coincide with the foam's strut system. However, the algorithm must be parametrised carefully to avoid segmentation errors. In the following, we provide a guideline to obtain optimal parameters for a given foam image.

II. Cell Reconstruction

Let us assume a digital image whose foreground represents the binarised strut system X of an open cell foam. According to our model assumption, the pore space X^c of the foam, i. e. the background of the image, is decomposed into the cells of a Laguerre tessellation $\mathcal{T}$. X itself is interpreted as the dilated edge system of $\mathcal{T}$.

Following [5], an approximation of $\mathcal{T}$ can be obtained by an image analytic cell reconstruction of the pore space using the watershed transformation. That means to partition the pore space into regions that are separated by interfaces known as watersheds. For the binarised strut system X of a foam, a partition of its cell system can be obtained by the following image processing chain:

1) Euclidean distance transform D_{X^c} on the pore space,
2) Euclidean distance transform D_X on the binarised strut system,
3) Combine both distance images such that $D = \big(D_{X^c} + \min(D_X)\big) - D_X$,
4) Invert D by computing its complement D^c,
5) Suppress superfluous minima (optional),
6) Watershed transform on D^c.

To guide the flooding process to the centres of the strut system, step 3 combines both distance images.

Note that while step 5 is theoretically optional, it is crucial to avoid over- and undersegmentation. For each regional minimum, a new cell is created by the watershed algorithm. Consequently, a cell may be *oversegmented* owing to a superfluous minimum in D, that is, it is separated by a spurious watershed. Conversely, a cell is called *undersegmented* if it is not marked by a minimum in D.

To get a correct segmentation, we may superimpose a set of markers on D such that each regional minimum represents the centre of one foam cell only (see [6, Sec. 6.3.6] for details). In contrast to approaches that remove superfluous minima by smoothing of D [6, Sec. 6.3.4] or by 'preflooding' the watershed transform [7], markers allow to correct for undersegmentation as well. Moreover, markers are independent of the actual implementation of the watershed transform and allow (manual or automated) corrections. Details to compute such markers are given below.

III. Construction of Markers

To obtain a set of markers that reconstructs each cell of a foam exactly by one labelled region, we assume the digitised dilated edge system X of a Laguerre tessellation $\mathcal{T}$. From the definition of the Euclidean distance map, it is easy to see that a local maximum near the centre of each cell of $\mathcal{T}$ exists. Hence, these maxima are promising candidates for markers. Note that this is actually the idea behind the cell reconstruction procedure outlined in the preceding section.

However, these maxima are generally not unique, and thus an additional filtering step is necessary. As the maxima lie near the centres of the cells, we may relate their values to the mean breadth of the corresponding cells. Hence, a filter for a whole foam should take into account the expected mean breadth $\bar{b}$ of the typical cell of the foam.

In practice, $\bar{b}$ can be obtained from the binarised strut system of a foam image by the approach proposed in [8]. Recall that the pore space of the foam corresponds to the cells of a Laguerre tessellation $\mathcal{T}$. Let us assume that the typical cell of $\mathcal{T}$ is, up to a scale factor k, distributed like the typical cell of a known reference Laguerre tessellation $\mathcal{M}$. Then by knowing k, we may obtain the mean value characteristics of $\mathcal{T}$ from $\mathcal{M}$.

To determine k, [8] exploits that the Euler characteristic χ_V of X and $\mathcal{M}$ are related by $\chi_V(X) = \chi_V(\mathcal{M})/k^3$, where the model $\mathcal{M}$ is normalised such that the volume of its typical cell equals one. The expected mean breadth of the typical cell of $\mathcal{T}$ can be obtained by $\bar{b}(\mathcal{T}) = k\bar{b}(\mathcal{M})$. For $\mathcal{M}$, [8] suggests the use of Laguerre tessellations generated from random dense sphere packings with a coefficient of variation (CV) of the sphere volume distribution of 0.2 and 2.0, or the Weaire–Phelan structure [9].

A filter that suppresses superfluous maxima can be constructed by dilating D_{X^c} with a cube whose edge length corresponds to the scaled expected mean breadth $\bar{b}$ of the typical cell of $\mathcal{T}$. More precisely that means $D = D_{X^c} \oplus s\bar{b}\mathrm{C}^3$, where $\oplus$ denotes the dilation operator, C^3 denotes the unit cube and $s \in \mathbb{R}_+$. Consequently, the connected components of the regional maxima of D are convex and lie within the cells of $\mathcal{T}$. Hence, their centres of mass (CMS) are markers for the cells of $\mathcal{T}$.

This procedure can be summarised in the following image processing chain:

1) Euclidean distance transform D_{X^c} on the pore space,
2) Dilate D_{X^c} with a cube of edge length $s\bar{b}$ using reflective boundary conditions,
3) Compute the regional maxima of the result from step 2,
4) The markers are the CMS of each connected component of the regional maxima.

Note the use of reflective boundary conditions in step 2 to avoid undersegmentation at the boundaries. For this correction to be effective, the reflective boundary should have at least the size of the structuring element used in the dilation step. But even in this case undersegmentation at the boundaries of the image cannot be completely avoided.

IV. Parameter Selection

To get an approximation of the optimal value for s, we used the following experimental setup: Consider a Laguerre tessellation with 1500 cells generated from a random dense sphere packing with lognormally distributed sphere volumes. Their CVs were varied from 0.2 to 2 in steps of 0.45. We then computed the corresponding markers using the real value of the expected mean breadth on the digitised edge system of the tessellations in a cube with edge length 1000.

As the exact shape of the cells is known, we may count the number of markers that fall within a given cell. For an optimal s, exactly one marker should fall in each cell. This means that the number of cells with missing or too many markers should be small. Hence, we may assess the overall segmentation error by the proportion of cells with none or more than one marker. However, as segmentation errors at the image boundaries cannot be completely avoided, we only considered cells that were kept by a suitable edge correction for the analysis like Miles' associated point rule [10].

In a pilot study that contained 15 realisations for each CV, we determined the interesting values for s in a range from 0.025 to 0.8. For s greater than 0.4, more than $50\,\%$ of the cells were undersegmented. Hence, we considered only values up to 0.4 and repeated the experiment another 15 times.

Fig. 1 summarises the results of all 30 runs for each CV. The optimal values for s are given in Table I. These were obtained by the intersection of the weighted least square fits to the proportion of under- and oversegmented cells in the experimental data. The amount of undersegmentation is described by $u(x) = ax^b$ and the amount of oversegmentation by $o(x) = c/(10x)^d$ with $a, b, c, d \in \mathbb{R}$ and $x \in \mathbb{R}$. In all cases the combined segmentation error was smaller than one percent.

To account for the influence of anisotropy, which is often found in real foams (see e. g. [11] and [12]), we repeated the experiment with models that exhibited a slight cell anisotropy. The cell anisotropy was incorporated by scaling the z-axis of the original models in steps of 0.1 from 0.7 to 1.3, which yields structures with oblate and prolate cells. The results for the optimal anisotropy scale parameters are also summarised in Table I.

For oblate cells the scale factors increase on average by approximately $8\,\%$. Conversely, for prolate ones the scale factors decrease in average by approximately $15\,\%$. However, the influence on the combined segmentation error is negligible. Even in the worst case the error did not exceed one percent when evaluated with respect to the appropriate isotropic models $u(x)$ and $o(x)$.

However, when we are dealing with real foams, the CV and the amount of anisotropy is usually unknown. Hence, we could not choose the optimal scale factor and risk to either use a scale factor that is smaller or bigger than the optimal one. In the first case oversegmentation and in the second one undersegmentation increases.

In practice, the mean isotropic scale factor of 0.11 has proven to avoid undersegmentation almost entirely. To correct oversegmentation caused by anisotropy at the image boundaries, additionally, the following heuristic can be used: Take all markers that are at least one half of the expected mean breadth $\bar{b}$ of the typical cell away from the image boundary, dilate them with a cube of edge length $\bar{b}/3$, and use the CMS of the remaining connected components as replacement for the original markers at the image boundary.

V. Conclusion

The image analytic cell reconstruction proposed in [5] is a common procedure to obtain the cell system of a foam. However, the parametrisation of the underlying watershed algorithm is not trivial. In this work, we suggest a marker based approach and provide a guideline to choose the optimal parameters. The result is a nearly perfect cell reconstruction with segmentation errors below one percent.

TABLE I
OPTIMAL SCALE PARAMETERS FOR THE EXPECTED MEAN BREADTH OF THE TYPICAL CELL WITH RESPECT TO UNDER- AND OVERSEGMENTATION.

AS*	Coefficient of Variation				
	0.2	0.65	1.1	1.55	2.0
0.7	0.1507	0.1665	0.1352	0.1147	0.0971
0.8	0.0983	0.1603	0.1313	0.1099	0.1048
0.9	0.0980	0.1378	0.1102	0.1060	0.1024
–	0.1028	0.1344	0.1090	0.0938	0.0930
1.1	0.0980	0.1288	0.1059	0.0904	0.0858
1.2	0.0980	0.1211	0.1024	0.0869	0.0828
1.3	0.0742	0.1147	0.1016	0.0838	0.0817

* Scale factor of the z-axis to achieve anisotropy.

Note that the introduced marker based procedure is not restricted to open cell foams. It can be readily applied to other cellular structures as it only uses the information of the Euclidean distance map on the pore space. A similar study for closed cell foams was conducted in [13], which uses manually segmented real foams as reference and a smoothing approach. Segmentation errors in between $7.5\,\%$ and $20\,\%$ were reported for an open cell polyurethane and a closed cell silicon carbide foam.

REFERENCES

[1] L. Gong, S. Kyriakides, and W.-Y. Jang, "Compressive response of open-cell foams. Part I: Morphology and elastic properties," *International Journal of Solids and Structures*, vol. 42, no. 5–6, pp. 1355–1379, 2005.

[2] N. J. Mills, "The high strain mechanical response of the wet Kelvin model for open-cell foams," *International Journal of Solids and Structures*, vol. 44, no. 1, pp. 51–65, 2007.

[3] W.-Y. Jang, A. Kraynik, and S. Kyriakides, "On the microstructure of open-cell foams and its effect on elastic properties," *International Journal of Solids and Structures*, vol. 45, no. 7–8, pp. 1845–1875, 2008.

[4] A. Liebscher, "Stochastic modelling of foams," Ph.D. dissertation, Fachbereich Mathematik, TU Kaiserslautern, 2014, iSBN 978-3-8396-0789-3.

[5] V. Cenens, R. Huis, B. Chauvaux, J. M. Dereppe, C. Gratin, and F. Meyer, "3d cellular structure characterization of flexible polyurethane foam," in *Cellular and microcellular materials*, V. Kumar and K. A. Seeler, Eds. ASME, 1994, vol. 53, pp. 29–44.

[6] P. Soille, *Morphological Image Analysis*. Springer, 2002.

[7] F. Meyer, "Levelings, image simplification filters for segmentation," *Journal of Mathematical Imaging and Vision*, vol. 20, no. 1–2, pp. 59–72, 2004.

[8] K. Schladitz, C. Redenbach, T. Sych, and M. Godehardt, "Model based estimation of geometric characteristics of open foams," *Methodology and Computing in Applied Probability*, vol. 14, no. 4, pp. 1011–1032, 2012.

[9] D. Weaire and R. Phelan, "A counterexample to Kelvin's conjecture on minimal surfaces," *Philosophical Magazine Letters*, vol. 69, pp. 107–110, 1994.

[10] R. E. Miles, "The sampling, by quadrats, of planar aggregates," *Journal of Microscopy*, vol. 113, no. 3, pp. 257–267, 1978.

[11] K. Kose, "3d NMR imaging of foam structures," *Journal of Magnetic Resonance*, vol. A118, no. 2, pp. 195–201, 1996.

[12] M. D. Montminy, A. R. Tannenbaum, and C. W. Macosko, "The 3d structure of real polymer foams," *Journal of Colloid and Interface Science*, vol. 280, no. 1, pp. 202–211, 2004.

[13] G. Schwarz, "Automatische bildanalytische zellrekonstruktion für pmi-hartschäume," Master's thesis, Fachbereich Mathematik, TU Kaiserslautern, 2012.

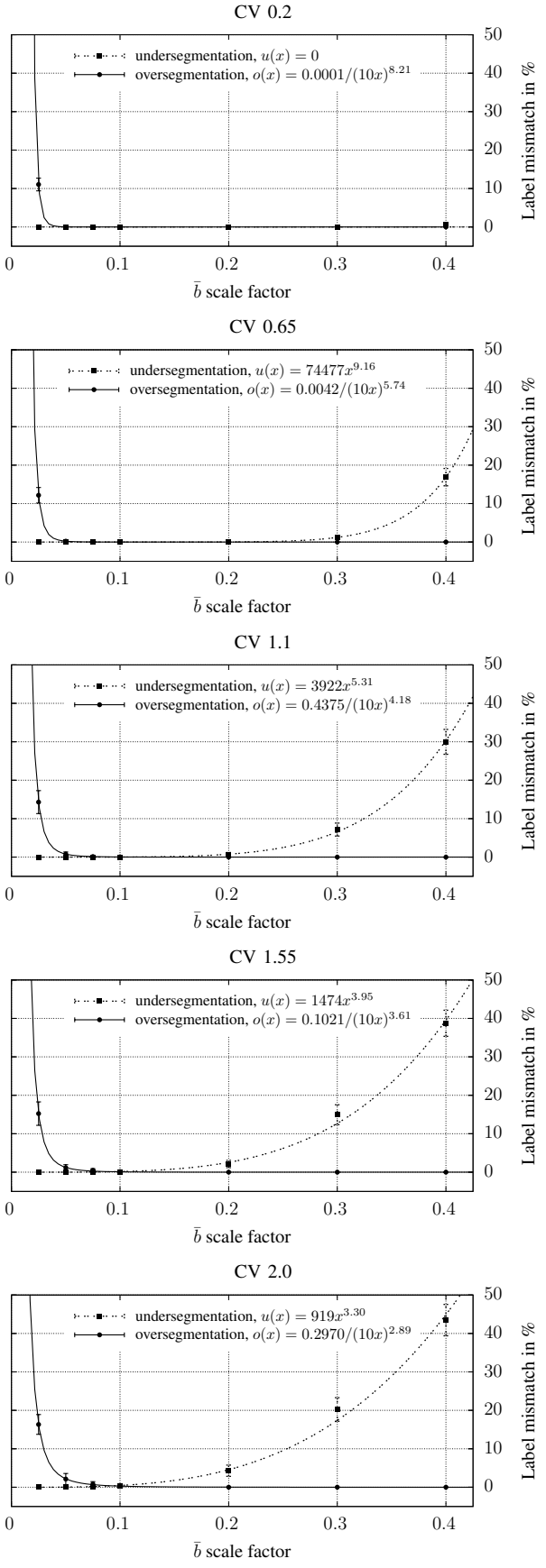

Fig. 1. Segmentation errors with respect to the scaling of the expected mean breadth $\bar{b}$. The results are averaged over 30 foam models for each coefficient of variation (CV) of the initial sphere volume distribution.